Developmental Biology 426 (2017) 84–96

Contents lists available at ScienceDirect

Developmental Biology

journal homepage: www.elsevier.com/locate/developmentalbiology

Original research article

Histone demethylases Kdm6ba and Kdm6bb redundantly promote cardiomyocyte proliferation during zebrafish heart ventricle maturation

Alexander A. Akerberg[a,b], Astra Henner[a], Scott Stewart[a], Kryn Stankunas[a,b,*]

[a] Institute of Molecular Biology, University of Oregon, Eugene, OR 97403-1229, United States
[b] Department of Biology, University of Oregon, Eugene, OR 97403-1229, United States

ARTICLE INFO

Keywords:
H3K27me3
Histone demethylase
Kdm6b
Cardiogenesis
Ventricle
Trabeculation

ABSTRACT

Trimethylation of lysine 27 on histone 3 (H3K27me3) by the Polycomb repressive complex 2 (PRC2) contributes to localized and inherited transcriptional repression. Kdm6b (Jmjd3) is a H3K27me3 demethylase that can relieve repression-associated H3K27me3 marks, thereby supporting activation of previously silenced genes. Kdm6b is proposed to contribute to early developmental cell fate specification, cardiovascular differentiation, and/or later steps of organogenesis, including endochondral bone formation and lung development. We pursued loss-of-function studies in zebrafish to define the conserved developmental roles of Kdm6b. *kdm6ba* and *kdm6bb* homozygous deficient zebrafish are each viable and fertile. However, loss of both *kdm6ba* and *kdm6bb* shows Kdm6b proteins share redundant and pleiotropic roles in organogenesis without impacting initial cell fate specification. In the developing heart, co-expressed Kdm6b proteins promote cardiomyocyte proliferation coupled with the initial stages of cardiac trabeculation. While newly formed trabecular cardiomyocytes display a striking transient decrease in bulk cellular H3K27me3 levels, this demethylation is independent of collective Kdm6b. Our results indicate a restricted and likely locus-specific role for Kdm6b demethylases during heart ventricle maturation rather than initial cardiogenesis.

1. Introduction

Covalent histone modifications establish chromatin landscapes that influence gene expression programs by promoting active or silenced transcriptional states. For instance, localized trimethylation of lysine 27 on histone 3 (H3K27me3) in vertebrates is deposited by Enhancer of zeste homolog 1 and 2 (Ezh1 and 2), the catalytic subunits of the Polycomb repressive complex 2 (PRC2), and is associated with gene silencing (Cao et al., 2002; Margueron and Reinberg, 2011; Müller et al., 2002). H3K27me3 marks can be removed by the lysine-specific demethylases Kdm6a (Utx) and Kdm6b (Jmjd3) (Cloos et al., 2008; Klose and Zhang, 2007; Mosammaparast and Shi, 2010). Therefore, H3K27me3 modifications likely provide an epigenetically inherited but reversible layer of transcriptional control. In vertebrates, H3K27me3 dynamics are implicated in cell fate specification (Alder et al., 2010; Dahl et al., 2010; Rugg-Gunn et al., 2010) and cell reprogramming associated with acquired pluripotency (Azuara et al., 2006; Bernstein et al., 2006; Mikkelsen et al., 2007). Further, vertebrate H3K27me3 demethylases directly support cell signal or transcription factor-induced gene expression programs (Jiang et al., 2013; Kartikasari et al., 2013; Ramadoss et al., 2012) and de-differentiation during organ regeneration (Stewart et al., 2009).

Studies using embryonic stem cells (ES cells) suggest Kdm6b enables cell specification of all three germ layers (Burgold et al., 2008; Kartikasari et al., 2013; Ohtani et al., 2011, 2013). These results predict that Kdm6b is responsible for relieving H3K27me3 marks at fate specifying genes as pluripotent cells adopt distinct cell lineage identities (Bernstein et al., 2006; Mikkelsen et al., 2007). However, in vivo tests of this model using mouse *Kdm6b* reverse genetics have yielded conflicting results. Mice homozygous for a *Kdm6b* allele that deletes exons encoding N-terminal regions of the protein are peri-implantation lethal at embryonic day 6.5 (E6.5) (Ohtani et al., 2013). In contrast, mice homozygous for several independently generated *Kdm6b* mutant alleles that delete the catalytic JmjC domain die perinatally with lung defects (Q. Li et al., 2014; Satoh et al., 2010; Shpargel et al., 2014; Zhang et al., 2015). These latter studies suggest that Kdm6b-driven H3K27me3 demethylation does not instructively derepress key cell fate regulatory genes during early embryonic development.

Kdm6b-deficient mouse embryos are smaller and edematous (Q. Li et al., 2014b), implicating Kdm6b in cardiovascular development. In further support, H3K27me3 marks are conspicuously lost from key

* Corresponding author at: Institute of Molecular Biology, University of Oregon, 273 Onyx Bridge, 1318 Franklin Blvd. Eugene, OR 97403-1229, United States.
E-mail address: kryn@uoregon.edu (K. Stankunas).

http://dx.doi.org/10.1016/j.ydbio.2017.03.030
Received 31 August 2016; Received in revised form 1 March 2017; Accepted 28 March 2017
Available online 01 April 2017
0012-1606/

cardiogenic genes during in vitro cardiac differentiation of ES cells (Paige et al., 2012; Wamstad et al., 2012) and PRC2 is required to maintain cardiomyocyte identity (Delgado-Olguín et al., 2012; He et al., 2012; San et al., 2016). Additionally, *Kdm6b*$^{-/-}$ ESCs induced to undergo cardiomyocyte differentiation misexpress many genes implicated in early heart development, including decreased levels of the cardiac progenitor factors *Mesp1*, *Pdgfra*, and *Mef2c* (Ohtani et al., 2011). Correspondingly, *Kdm6b*-deficient ES cells exhibit reduced ability to form differentiated cardiomyocytes and contractile embryoid bodies (EBs). Although in vivo mouse and zebrafish studies demonstrate Kdm6a contributes to the activation of core cardiac transcription factors (Lee et al., 2012; Van Laarhoven et al., 2015; Welstead et al., 2012), the in vivo contributions of Kdm6b to cardiovascular development have not been examined.

We pursued in vivo loss-of-function studies in zebrafish to define the evolutionarily conserved contributions of *Kdm6b* to vertebrate development. Due to an ancestral whole genome duplication in the teleost lineage (Amores, 1998; Jaillon et al., 2004; Meyer and Schartl, 1999), the zebrafish genome contains two *Kdm6b* orthologs, *kdm6ba* and *kdm6bb*. In such instances of duplicated genes, the "ohnologs" frequently acquire distinct roles or one ohnolog becomes non-functional due to relaxed selective pressure (Force et al., 1999; Lynch and Force, 2000; Postlethwait, 2007; Steinke et al., 2006). However, redundant functions, with or without compensatory networks, are also possible. While *kdm6bb* may support the reactivation of embryonic developmental gene programs during fin regeneration (Stewart et al., 2009), *kdm6ba* has not been studied in any context.

We generated *kdm6ba* and *kdm6bb* loss-of-function alleles using CRISPR/Cas9 mutagenesis. Zebrafish homozygous for either individual allele are viable and fertile. However, *kdm6ba*$^{-/-}$; *kdm6bb*$^{-/-}$ zebrafish larvae have pleiotropic yet specific organogenesis defects, including a small heart ventricle, consistent with coinciding heart expression. The small ventricle originates from insufficient proliferation of both endocardial and myocardial cells associated with the initiation of cardiac trabeculation at larval hatching. This burst of trabecular cardiomyocyte proliferation correlates with transient bulk cellular H3K27me3 demethylation, implying a global relaxing of gene repression enables the cell cycle entry transition. However, collective Kdm6b does not appear to promote this observed cell-wide demethylation and therefore likely has locus-specific roles. Our data provide an example of straightforward non-compensatory redundancy between duplicated genes in zebrafish. Further, we show that Kdm6b's unique functions (those not shared with Kdm6a) are largely restricted to later stages of organ growth and morphogenesis rather than early cell fate specification or progenitor cell activity.

2. Materials and methods

2.1. Zebrafish

The University of Oregon Institutional Animal Care and Use Committee (IACUC) approved and monitored all zebrafish procedures following the guidelines and recommendations outlined by the Guide for the Care and Use of Laboratory Animals (National Academic Press). Wildtype AB, *Tg(myl7:dsRedExpress-nuc)* (Takeuchi et al., 2011), and *Tg(kdrl:EGFP)* (Jin et al., 2005) lines were used in this study.

2.2. CRISPR-Cas9 generation of mutant alleles

CRISPR-Cas9-mediated mutagenesis was used to generate targeted deletions within the JmjC domains of both *kdm6ba* and *kdm6bb*. Guide RNAs (gRNAs) were generated following methods adapted from (Bassett et al., 2013). Guide oligonucleotides were obtained from Integrated DNA Technologies and had the following core sequence: 5'-AATTAATACGACTCACTATA-NNNNNNNNNNNNNNNNNNN-GTTTTAGAGCTAGAAATAGC-3', with a T7 promoter sequence followed by a series of Ns indicating the targeting sequence. The gRNA targeting sequences for *kdm6ba* and *kdm6bb* were 5'-GCTTAGCATATTCCCACTGG-3' and 5'-CAGGTGGAAGGC-GCAGTTGC-3', respectively. Guide oligonucleotides were annealed to a generic gRNA scaffold (5'-GATCCGCACCGACTCGGTGCCACTTTTTCAAGTTGATAACGGACT-AGCCTTATTTTAACTTGCTATTTCTAGCTCTAAAAC-3') and extended using Phusion polymerase (New England Biolabs) followed by column-based purification.

In vitro transcription of gRNAs was performed using the Megascript T7 Transcription Kit (Thermo Fisher) and purified via RNA Clean & Concentrator columns (Zymo Research). Cas9 mRNA was in vitro transcribed from Addgene plasmid 46757:pT3TS-nCas9n (Jao et al., 2013) using the T3 mMessage mMachine kit (Thermo Fisher). Cas9 mRNA and gRNA were combined and diluted to a final concentration of 100 ng/μl in Danieau's buffer containing phenol red. We injected 1–3 nl of the Cas9/gRNA mix into the developing embryo at the one-cell stage. Fish raised from injected embryos (see below) were screened for mutations by amplicon sequencing. Founders carrying isolated mutant alleles were outcrossed to wildtype fish to isolate stable germline transmitting lines used for subsequent crosses and phenotypic analyses.

2.3. Genotyping kdm6ba and kdm6bb mutant alleles

The *kdm6ba* allele was assessed by PCR using primers 5'-TGGCACAAACATTGACCTGT-3' and 5'-CATCATGGACAGCAAACCAC-3' followed by restriction digest with NcoI (New England Biolabs). The *kdm6bb* mutant allele was assessed by PCR using primers 5'-CTCAAAGCAGAAAGCTGTTGG-3' and 5'-GTGTGGCCAACATGACTCAG-3'.

2.4. In situ hybridization

In situ hybridization probes were synthesized from PCRII-based plasmids (Life Technologies) containing cloned cDNA amplicons. PCR products were obtained from pooled samples of embryonic zebrafish cDNA using the following primers: *kdm6bb* 5'-CCACTTGACCAACTGCCTTGCAAAAC-3', 5'-CTGAAAACACACTCCGAGAGGTATCGC-3'; *kdm6ba* 5'-TGGCACAAACATTGACCTGT-3', 5'- GTGTGAGGGAAAGGGATGAG-3'. Plasmids were linearized by digestion with NotI and BamHI, respectively. Digoxigenin-11-dUTP (Roche) labeled RNA synthesis was performed using Sp6 (for *kdm6bb* probe) or T7 (for *kdm6ba* probe). DIG-labeled probes were DNase treated prior to LiCl precipitation and then resuspended in RNase/DNase free water. Whole-mount in situ hybridizations were performed as described (Thisse and Thisse, 2008). Hybridized embryos were blocked with 5% normal goat serum in phosphate-buffered saline (PBS) and then incubated overnight with alkaline phosphatase-conjugated anti-DIG antibody (Roche) diluted 1:1000 in blocking buffer. Embryos were developed at room temperature using NBT/BCIP (Promega) and then dehydrated into 100% methanol and stored at −20 °C. Embryos were then rehydrated and allowed to equilibrate in 100% glycerol at 4 °C prior to imaging on a Leica M165 FC stereomicroscope.

2.5. Whole mount immunofluorescence and imaging

Anti-GFP (AVES) immunostaining was performed as described (Akerberg et al., 2014). Staining for cardiac troponin (CT3, Developmental Studies Hybridoma Bank), DsRed (Clontech) and S46 (Developmental Studies Hybridoma Bank) was performed using a protocol adapted from (Zhou et al., 2011). Embryonic hearts were arrested in diastole with 0.5 M KCl and fixed overnight at 4 °C in phosphate-buffered saline (PBS) containing 4% paraformaldehyde. The following day, embryos were washed in PBS and dehydrated through a methanol series. Embryos in 100% methanol were stored at −20 °C for at least 24 h prior to rehydration into PBS containing 0.1% Tween-20 (PBST). Embryos were then blocked with PBS containing 1% BSA, 1%

Triton X-100, 0.1% DMSO for four hours. Embryos were incubated with primary antibodies diluted in block solution for 4–5 h at room temperature with gentle agitation followed by three 20' washes in PBS containing 0.5% Triton X-100 (PB0.5X). Alexa-conjugated secondary antibodies (Thermo Fisher) were diluted 1:1000 in PB0.5X and incubated with embryos for 2–3 h at room temperature with gentle agitation. Lastly, embryos were washed and stored in TBST (20 mM Tris pH 7.5, 150 mM NaCl, 0.5% Triton X-100) prior to imaging. Primary antibodies CT3, DsRed, and S46 were used at dilutions of 1:500, 1:500, and 1:250, respectively. Immunostained embryos as well as transgenic embryos with native fluorescence were mounted in low melt agarose and imaged with a Leica M165 FC stereomicroscope, Nikon Eclipse Ti inverted fluorescence microscope, or Leica SD6000 spinning disk confocal microscope. 10x DIC images were acquired using a Nikon Eclipse Ti inverted microscope and stitched together using NIS Elements Advanced Research software.

2.6. Live embryo imaging

Embryos of the desired stage were anesthetized in Tricaine (Western Chemical) and immobilized in 0.75% low melt agarose dissolved in embryo media (EM). Embryos were imaged on a glass bottom FluoroDish (World Precision Instruments) using epifluorescence or DIC optics with a Nikon Eclipse Ti inverted microscope.

2.7. Cell counting and morphometrics

Cardiomyocyte quantification was performed on *Tg(myl7:dsRed-nuc)* transgenic embryos that first were fixed overnight in PBS containing 4% paraformaldehyde. Embryos were then immediately antibody stained for dsRed and CT3. Stained embryos were mounted in low melt agarose after their heads were removed to provide an unobstructed view of the heart. Mounted embryos were imaged with a Leica SD6000 spinning disk confocal microscope. Image stacks were processed and nuclei counted using ImageJ (National Institutes of Health). Area measurements of trabeculated muscle located between OFT and the atrioventricular canal (AVC) used ImageJ measurement tools. Trabeculation index values were calculated as the ratio between the length of the interior (trabecular) and exterior of the ventricle. Individual data points were normalized to the mean of respective clutch mate control samples.

2.8. Skeletal staining

Alcian Blue staining of zebrafish larvae was performed as described (Walker and Kimmel, 2007) with subsequent imaging using a Leica M165 FC stereomicroscope (whole mount) or Leica DM4000B upright microscope (flat mount).

2.9. Histological sectioning and immunostaining

Paraffin sections were processed following procedures used for dissected mouse hearts (Akerberg et al., 2015). Hematoxylin and eosin staining on paraffin sections was performed using conventional reagents and methodology (Ricca Chemical Company). For immunostaining paraffin sections, slides were de-paraffinized using Xylenes and rehydrated into distilled water using a series of graded ethanol washes. Antigens were retrieved by either 1) pressure-cooking for 10' in 1 mM EDTA and 0.1% Tween-20 (CT3, PCNA (Sigma), myosin heavy chain (MF20, Developmental Studies Hybridoma Bank), GFP, and DsRed antibodies) or 2) 10' incubation in 0.25% trypsin solution (H3K27me3 antibody, Millipore). Slides were blocked for 1 h with 10% dried milk, 0.1% Tween-20 or 10% normal goat serum (for anti-H3K27me3) in PBS. Primary antibodies were diluted 1:500 (or 1:50 for MF20) in their respective block solutions and incubated overnight at 4 °C. Slides were then washed 5×10' in PBST (1x PBS with 0.1% Tween-20) and incubated with Alexa-conjugated secondary antibodies diluted 1:1000 in block solution for 1 h. After 3×10' PBST washes, the slides were submerged for 5' in Hoechst diluted 1:5000 in PBST. Slides were washed in PBST and mounted with Fluorogel (Electron Microscopy Sciences). Imaging was performed with a Leica upright fluorescent microscope or either an Olympus Fluoview FV1000 or Zeiss LSM 880 laser scanning confocal microscope.

2.10. 5-ethynyl-2-deoxyuridine labeling

Fish were incubated with 5-ethynyl-2-deoxyuridine (EdU) (Thermo Fisher) at a concentration of 0.1 mg/ml in embryo media for 12–15 h prior to harvest at 5 dpf. Embryos were processed into paraffin sections as described above. EdU Click-It reactions (Thermo Fisher) were performed prior to immunostaining with the samples kept in the dark throughout subsequent staining procedures.

2.11. Quantitative reverse transcription polymerase chain reaction (qRT-PCR)

cDNA was synthesized using SuperScript III (Thermo Fisher) with Trizol-isolated RNA harvested from pooled embryos (5–10 embryos per pool) or dissected embryonic hearts. qRT-PCR was performed using KAPA SYBR FAST qPCR master mix reagents (Kapa Biosystems). Relative mRNA expression was normalized using *rpl18* or *rps11* to calculate ΔCTs (threshold cycles). Transcript levels were compared using a ΔΔCT approach. ΔCT values were used for two-tailed Student's *t*-tests to determine significance with a Bonferroni correction for multiple comparisons. qPCR primer sequences: *kdm6bb* 5'-GCATGGCGTGGACTATCTG-3', 5'-CGTGAATCATAGGGACGATTG-3'; *kdm6ba* 5'-GCCCAAACCTCTCCAATGTA-3', 5'-GTGTGAGGGAAAGGGATGAG-3'; *kdm6a* 5'-ACATAAACATTGGCCCTGGA-3', 5'-GCCACCAAGATCCCATTAGA-3'; *kdm6al* 5'-CACAACAACTTCTGCGCTGT-3', 5'-CCTCGTACAGGTCCTCCAGA-3'; *rpl18* 5'- CCGAGACCAAGAAATCCAGA-3', 5'- GAGGCCAGCAGTTTCTCTTG-3'; *rps11* 5'-GATGGCGGACACTAGAAC-3', 5'-CCAATCCAACGTTTCTGTGA -3'; *vmhcl* 5'-GATGGAACTGAGGATGCTGAC -3', 5'-TTGACTCTTGGATGGCACAG -3'.

3. Results

3.1. Histone demethylases kdm6ba and kdm6bb have non-compensatory redundant functions during zebrafish development

We monitored embryonic expression of the *kdm6b* H3K27me3 histone demethylase ohnologs by RNA in situ hybridization (Fig. 1A-J). *kdm6ba* transcripts were uniquely maternally contributed (Fig. 1F) whereas both *kdm6ba* and *kdm6bb* transcripts were robustly expressed in the developing brain (Fig. 1B-C and G-H), otic vesicles (Fig. 1C and H), and heart (Fig. 1D-E and I-J). The grossly similar expression patterns of *kdm6ba* and *kdm6bb* during early development suggested redundancy. Therefore, we generated mutant alleles of both genes using CRISPR/Cas9 targeted mutagenesis to investigate their unique and shared roles during zebrafish development.

We first targeted insertion-deletion (indel) mutations to the 5' end of the essential catalytic JmjC domain of *kdm6bb* (De Santa et al., 2007; Lan et al., 2007; Hong et al., 2007; Xiang et al., 2007), isolating a germline-transmitted allele (*kdm6bb*^{b1307}, abbreviated *kdm6bb*$^{-}$ from here forth) harboring a 40 bp deletion spanning the first 14 bp of exon 15 (Fig. 2A). This deletion introduces an early stop codon predicted to result in a truncated Kdm6bb protein lacking the entire JmjC domain. *kdm6bb*$^{-/-}$ fish did not exhibit any overt developmental defects and were both viable and fertile as adults (Fig. 2B-E). Vascular organization was also unchanged in *kdm6bb*$^{-/-}$ embryos at 3 dpf as visualized by the *Tg(kdrl:EGFP)* reporter line (Fig. S1A, B). Notably, *kdm6bb* transcript levels were decreased nearly nine fold in homozygous *kdm6bb*$^{-/-}$

animals at 30 h post fertilization (hpf) presumably due to nonsense mediated decay, as shown by qRT-PCR and in situ hybridization (Fig. 2F-H). Expression levels of the other three Kdm6-family demethylases *kdm6ba*, *kdm6a*, and *kdm6al* were not significantly different in *kdm6bb*$^{-/-}$ animals. Therefore, genetic deficiency of *kdm6bb* does not trigger transcriptional compensation (Fig. 2F).

We subsequently isolated a *kdm6ba* mutant allele (*kdm6ba*^{b1308}, henceforth denoted *kdm6ba*$^{-}$) containing a single base deletion within exon 14 of *kdm6ba* (Fig. 2I). This frameshift mutation is predicted to result in an early stop codon yielding a truncated Kdm6ba protein missing the JmjC domain. *kdm6ba*$^{-/-}$ embryos lacking the notable maternal contribution (*kdm6ba*^{MZ}) showed no overt embryonic defects at 24 and 48 hpf and were both viable and fertile (Fig. 2J-M). *kdm6ba*$^{-/-}$ embryos also exhibited normal vascular development at 3 dpf (Fig S1C, D). *kdm6ba*^{MZ} animals expressed three fold less *kdm6ba* mRNA than their wildtype clutchmates (Fig. 2N), likely reflecting nonsense mediated decay and further signifying *kdm6ba* loss of function. qRT-PCR showed that *kdm6ba*-deficiency did not elicit compensatory expression of *kdm6bb*, *kdm6a*, or *kdm6al* at 30 hpf (Fig. 2N).

To determine if the H3K27me3 demethylases *kdm6ba* and *kdm6bb* have redundant functions, we generated *kdm6ba*$^{-/-}$; *kdm6bb*$^{-/-}$ double mutant (or *kdm6b*-deficient) animals. Although *kdm6ba*$^{-/-}$; *kdm6bb*$^{-/-}$ fish developed normally for their first three days (Fig. S2A-D), they failed to inflate their swim bladder upon hatching and were not viable past 10–12 dpf (Fig. 3A-E). *kdm6b*-deficient larvae also consistently exhibited cardiac edema (Fig. 3D-D') and a craniofacial "slack jaw" abnormality in which the jaw was unable to close (Fig. 3D-D'). *kdm6ba*$^{-/-}$; *kdm6bb*$^{+/-}$ animals also failed to develop a swim bladder and did not survive to adulthood (Fig. 3C and E). Conversely, *kdm6ba*$^{+/-}$; *kdm6bb*$^{-/-}$ animals were completely viable with no obvious embryonic defects (Fig. 3B and E). This weighted dose-dependency suggests that Kdm6ba contributes relatively more to its and Kdm6bb's shared developmental roles, possibly explained by three-fold higher transcript levels of *kdm6ba* over *kdm6bb* at 30 hpf (Fig. 3F).

A further analysis of 5 dpf *kdm6ba*$^{-/-}$; *kdm6bb*$^{-/-}$ larvae revealed several additional defects. *kdm6b*-deficient animals exhibited cranial swelling arising between 4 and 5 dpf (Fig. 3G-H). Hematoxylin and eosin (H & E) staining of paraffin sections confirmed an intact but uninflated swim bladder in *kdm6ba*$^{-/-}$; *kdm6bb*$^{-/-}$ larvae (Fig. 3I-J). As Kdm6b promotes endochondral bone formation in mice (Zhang et al., 2015), we performed Alcian Blue staining to determine if *kdm6b*-deficient larvae exhibited abnormal cartilaginous bone. Whereas the majority of craniofacial skeletal development was unaffected, *kdm6ba*$^{-/-}$; *kdm6bb*$^{-/-}$ larvae displayed a truncated basihyal cartilage at 5 dpf and 7 dpf that likely accounts for the "slack-jaw" phenotype (Fig. 3K-P). By H & E staining of 7 dpf larvae, we found that the reduced basihyal in *kdm6b*-deficient larvae contained subjectively fewer but morphologically normal chondrocytes and retained associated ligaments (Fig. 3Q-T). These phenotypes and the larval stage lethality of *kdm6ba*$^{-/-}$; *kdm6bb*$^{-/-}$ fish are congruent with those mouse studies that proposed *Kdm6b* largely functions during later stages of organogenesis, rather than during early cell lineage specification (Burgold et al., 2012; Q. Li et al., 2014; Satoh et al., 2010; Shpargel et al., 2014; Zhang et al., 2015).

3.2. Kdm6b proteins promote larval stage cell proliferation associated with heart ventricle trabeculation

The absence of embryonic phenotypes in *kdm6ba*$^{-/-}$; *kdm6bb*$^{-/-}$

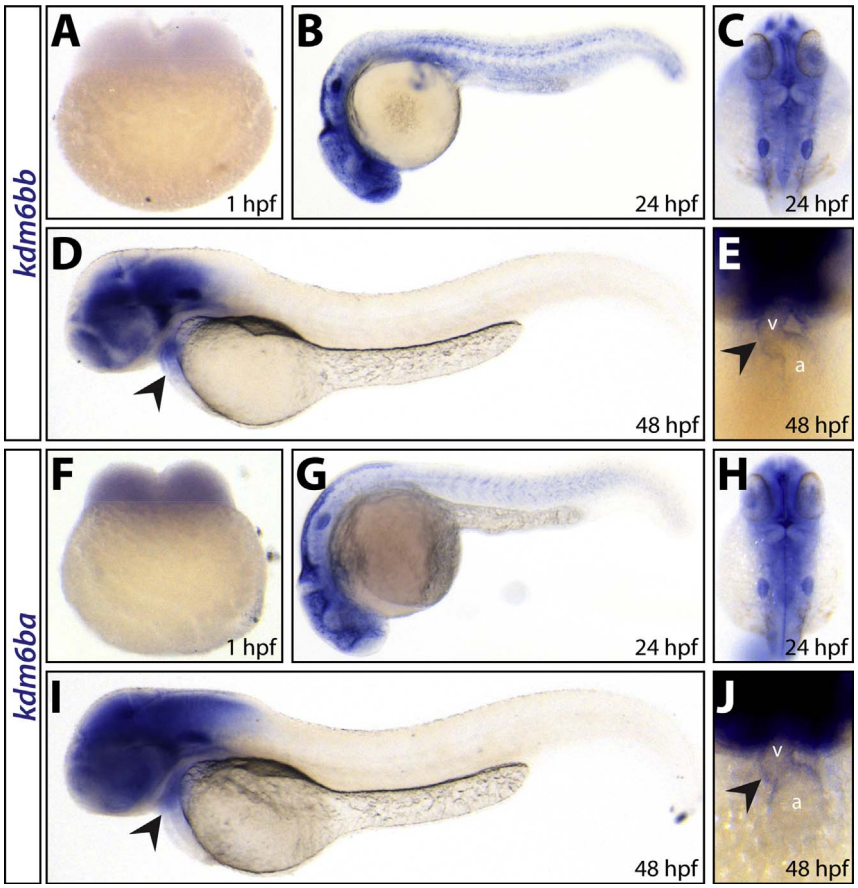

Fig. 1. *kdm6ba* and *kdm6bb* have broad and largely overlapping developmental expression patterns. (A-J) Whole mount in situ hybridization for *kdm6bb* (A-E) and *kdm6ba* (F-J) transcripts on 1 hpf (A and F), 24 hpf (B, C, G, H) and 48 hpf (D, E, I, J) embryos. Arrowheads denote cardiac expression. Abbreviations: a, atrium; v, ventricle.

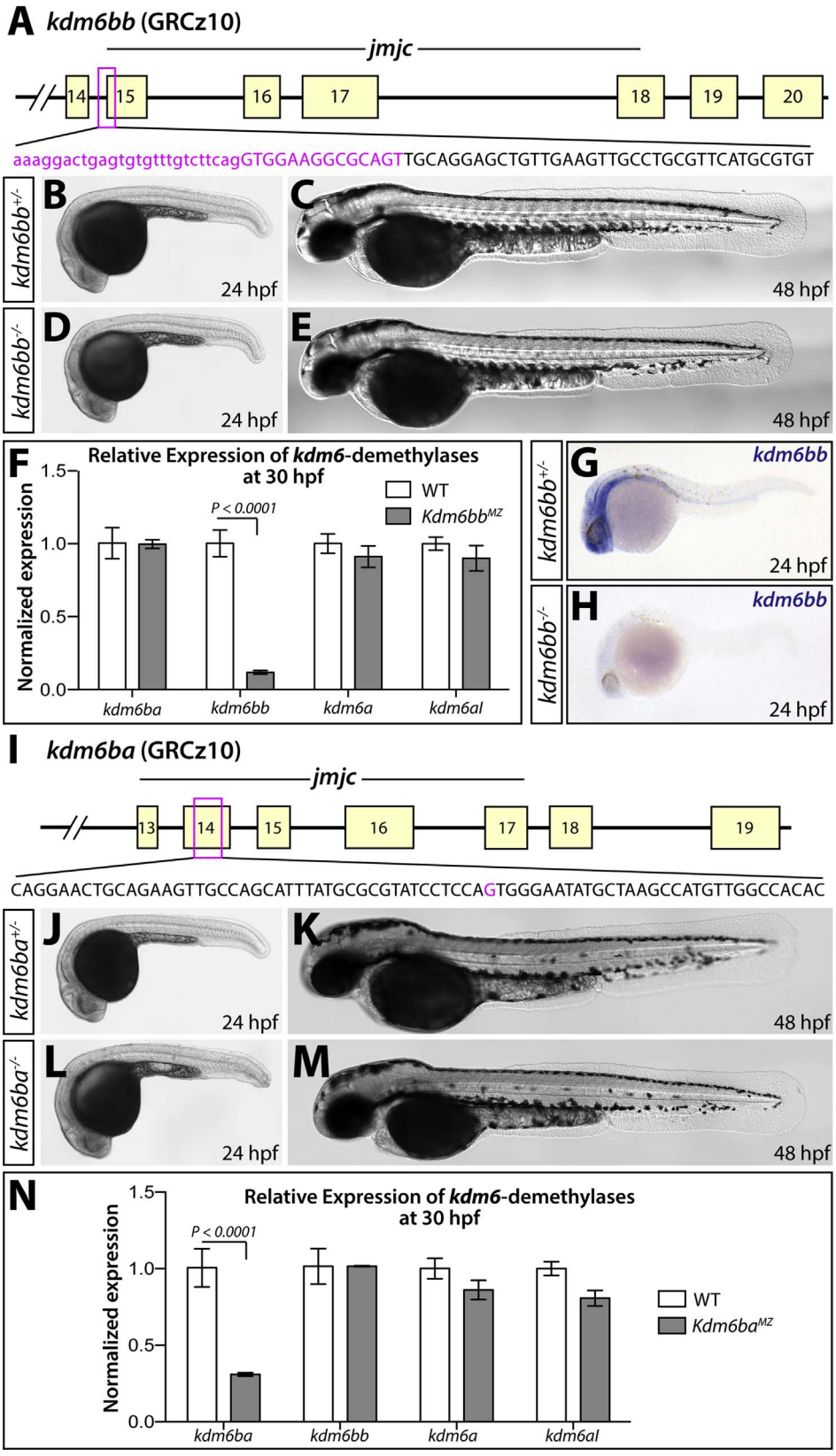

Fig. 2. Generation and characterization of *kdm6b* loss of function alleles. (A) Schematic showing the deleted sequence in the *kdm6bb* mutant allele recovered from CRISPR/Cas9 targeted mutagenesis (magenta bases). (B-E) Whole mount differential interference contrast (DIC) microscopy images of 24 (B and D) and 48 hpf (C and E) embryos. (F) Bar graph showing relative *kdm6bb* transcript levels between wildtype and *kdm6bb*^{MZ} embryos at 30 hpf determined by qRT-PCR on cDNA from three separate pools of ten embryos each. (G, H) In situ hybridization for *kdm6bb* on control and *kdm6bb*^{MZ} 24 hpf zebrafish embryos. (I) Schematic showing the CRISPR/Cas9-generated *kdm6ba* mutant allele. The deleted base is shown in magenta. (J-M) DIC images of control and *kdm6ba*^{MZ} embryos at 24 hpf (J and L) and 48 hpf (K and M). (N) Bar graphs comparing qRT-PCR-determined normalized expression levels of each H3K27me3 demethylase-encoding transcripts between 30 hpf wildtype and *kdm6bb*^{MZ} embryos (three independent pools of ten embryos each). Error bars in the bar graphs (F, N) show one standard deviation. P-values indicate a significant difference determined by Student's two-tailed *t*-tests after applying a Bonferroni correction for multiple comparisons.

embryos does not eliminate the possibility that maternally contributed mRNA or protein contribute to early lineage specification (Burgold et al., 2008; Kartikasari et al., 2013; Ohtani et al., 2013, 2011). Although the lethality of *kdm6ba*$^{-/-}$; *kdm6bb*$^{-/-}$ animals precluded us from eliminating maternal contributions of both transcripts, only *kdm6ba* transcripts were present prior to zygotic genome activation (Fig. 1A and F). To achieve maximum *kdm6b* depletion in the early embryo with respect to both maternal and zygotic contributions, we crossed *kdm6ba*$^{-/-}$; *kdm6bb*$^{+/+}$ females to *kdm6ba*$^{+/-}$; *kdm6bb*$^{-/-}$ males. *kdm6ba*^{MZ}; *kdm6bb*$^{+/-}$ progeny from this cross were phenotypically indistinguishable from *kdm6ba*$^{-/-}$; *kdm6bb*$^{+/-}$ animals, lacking a swim bladder and dying as larvae. Further, *kdm6ba*^{MZ}; *kdm6bb*$^{+/-}$ larvae did not develop the severe edema and slack-jaw phenotype seen in *kdm6ba*$^{-/-}$; *kdm6bb*$^{-/-}$ fish with intact maternal but not zygotic *kdm6ba* (Fig. S3A-C). Therefore, *kdm6b* demethylases likely do not have unique early embryogenesis roles necessitating maternally contributed mRNA or protein.

Despite the lack of embryonic cardiovascular phenotypes, the presence of cardiac edema in 5 dpf *kdm6ba*$^{-/-}$; *kdm6bb*$^{-/-}$ larvae implied Kdm6b demethylases are involved in cardiovascular development. The *Tg(kdrl:EGFP)* vascular-marking transgene showed that 3 dpf *kdm6ba*$^{-/-}$; *kdm6bb*$^{-/-}$ larvae have grossly normal aortic arch artery development (Fig. 4A and C). Likewise, cardiogenesis through 3 dpf, including the generation of *Tg(myl7:DsRed-nuc)*-marked cardiomyoctes, was unaffected by *kdm6b* deficiency (Fig. 4B and D-E). Live imaging revealed that hearts of *kdm6b*-deficient 5 dpf larvae produced unidirectional and steady blood flow, consistent with their normal OFTs and OFT valves (Movie S1, Fig. 4F-G). However, *kdm6ba*$^{-/-}$; *kdm6bb*$^{-/-}$ larvae had smaller and more spherically-shaped ventricles, which was also apparent by whole mount staining for cardiac troponin (CT3) and DsRed in a *Tg(myl7:DsRed-nuc)* background (Fig. 4H-I). To further characterize ventricle morphology in *kdm6b*-deficient animals, we analyzed H & E stained sagittal sections of 5 and 7 dpf larvae. 5 dpf *kdm6ba*$^{-/-}$; *kdm6bb*$^{-/-}$ larvae had a smaller and more rounded ventricle with greatly reduced number and size of trabecular projections that normally form on the outer curvature of the zebrafish ventricle between 3 and 4 dpf (Liu et al., 2010) (Fig. 4J-K). The OFT, atria, and atrioventricular canal (AVC) valves were notably unaffected. The specific trabeculation defect was even more apparent at 7 dpf (Fig. 4L-M). Quantitatively, *kdm6b*-deficient larvae first showed diminished trabeculation at 5 dpf followed by reduced ventricular muscle at 7 dpf (Fig. 4N, O, Fig. S4). Both *kdm6ba* and *kdm6bb* were robustly expressed in isolated 3.5 dpf hearts as determined by qRT-PCR (Fig. 4P). We conclude that *kdm6ba* and *kdm6bb* share a specific and heart autonomous role promoting early stages of zebrafish cardiac trabeculation.

By immunostaining sectioned larvae, we found that myosin heavy chain (recognized using the pan-myocardial MF20 antibody) and S46 (atrial cardiomyocyte-specific) were expressed normally in 5 dpf *kdm6ba*$^{-/-}$; *kdm6bb*$^{-/-}$ larval hearts (Fig. 5A-D'). Therefore, the diminished cardiac trabeculation in *kdm6b*-deficient larvae did not reflect an altered chamber identity. CT3 antibody staining further confirmed that ventricular cardiomyocytes of *kdm6*-deficient larvae were differentiated and formed myofibrils (Fig. 5B-B' and D-D'). Finally, we used the Tg(*kdrl:EGFP*) reporter line and anti-GFP staining to determine that the endocardium of *kdm6b*-deficient embryos was present and

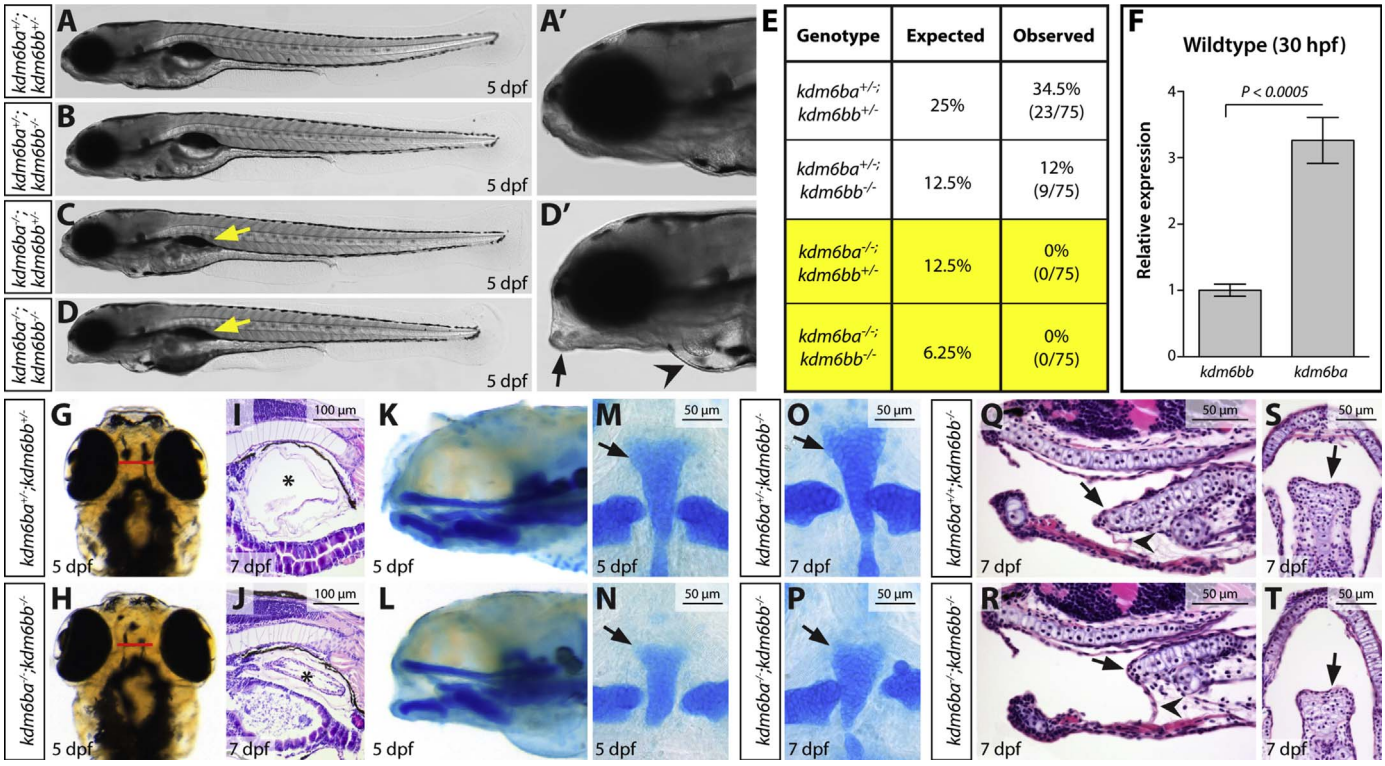

Fig. 3. Combined genetic deficiency of *kdm6ba* and *kdm6bb* causes pleiotropic larval development defects. (A-D) Whole mount stitched DIC microscopy images of clutch mate 5 dpf larvae of the indicated genotypes. (A' & D') Zoomed anterior region of the control and *kdm6ba*$^{-/-}$; *kdm6bb*$^{-/-}$ fish shown in A and D, respectively. Yellow arrows mark the absence of an inflated swim bladder. The black arrow and black arrowhead highlight the slack jaw and cardiac edema phenotypes, respectively, of a *kdm6ba*$^{-/-}$; *kdm6bb*$^{-/-}$ larvae. (E) Viability table showing the expected versus observed adult genotype frequencies from *kdm6ba*$^{+/-}$; *kdm6bb*$^{+/-}$ in-crosses. (F) Bar graph displaying relative *kdm6ba* and *kdm6bb* transcript levels in 30 hpf wildtype embryos. Data is normalized to *rpl18* expression. P-value is from a Student's two-tailed *t*-test with error bars showing one standard deviation. (G, H) Whole mount dorsal view of 5 dpf control and clutch mate *kdm6ba*/*kdm6bb*-deficient larvae. (I, J) H & E-stained sagittal sections through 7 dpf larvae centered on the swim bladder (asterisk). (K, L) Sagittal whole mount view of alcian blue stained 5 dpf larvae. (M-P) Flat mounts of alcian blue-stained 5 dpf (M, N) and 7 dpf (O, P) larvae of the indicated genotypes. Black arrows mark the basihyal cartilage. (Q-T) H & E-stained sagittal (Q, R) and coronal (S, T) midline sections through 7 dpf *kdm6bb*-null and *kdm6ba*/*kdm6bb*-double deficient larvae. Arrows indicate the basihyal cartilage and arrowheads point at the cartilage's associated ligament. 50 or 100 μm scale bars are shown.

maintained an epithelial organization (Fig. 5E'-F'). Collectively, these results show that Kdm6b is not required for the specification or differentiation of endocardial and myocardial cells and therefore that the trabeculation defects in *kdm6b*-deficient larvae likely represents a direct role of Kdm6b in trabecular growth and/or morphogenesis.

Myocardial proliferation around the time of larval hatching is required for the initiation of trabeculation in zebrafish (Liu et al., 2010). To determine if cardiac proliferation was impaired in *kdm6ba*$^{-/-}$; *kdm6bb*$^{-/-}$ larvae, we immunostained sections for proliferating cell nuclear antigen (PCNA), a marker of cycling cells (Fig. 5E-F'"). *kdm6b*-deficient animals displayed a near 50% reduction of both PCNA positive endocardial and myocardial cells at 5 dpf (Fig. 5G). This decrease in proliferative ventricular cells in *kdm6ba*$^{-/-}$; *kdm6bb*$^{-/-}$ larvae was especially striking using EdU incorporation assays to monitor cells that passed through S-phase between 4 and 5 dpf (Fig. 5H and I). In contrast, the normal number of cardiomyocytes in 72 hpf *kdm6ba*$^{-/-}$; *kdm6bb*$^{-/-}$ fish (Fig. 4B-E) suggests that embryonic cardiac proliferation was not disrupted in the absence of Kdm6b. We conclude that *kdm6bb* and *kdm6ba* redundantly promote trabecular outgrowth by enabling the coordinated endo- and myocardial proliferation that accompanies the larval stage initiation of trabeculation.

3.3. Transient global H3K27me3 demethylation in cardiomyocytes at the onset of myocardial trabeculation

H3K27me3 levels dramatically increase upon cardiomyocyte differentiation in mice (Delgado-Olguín et al., 2012). Therefore, Kdm6b likewise could regulate widespread rather than locus-specific changes in H3K27me3 levels during heart ventricle maturation. To assess this possibility, we first immunostained sections of 2.5, 3.5, and 5 dpf wildtype zebrafish with anti-H3K27me3 antibodies. Strikingly, H3K27me3 levels varied widely between different cardiac cell types and through the developmental course (Fig. 6). Endocardial cells consistently had very low H3K27me3 levels at 2.5 dpf that progressively increased from 3.5 to 5 dpf. In contrast, the flat nuclei of presumptive epicardial cells (first seen at 3.5 dpf and lacking associated myosin heavy chain immunoreactivity) had high H3K27me3 levels. At 2.5 dpf, prior to trabeculation, all cardiomyocytes displayed robust H3K27me3 levels. However, at 3.5 dpf, newly derived trabecular myocardial cells adjacent to the ventricular cavity frequently showed reduced bulk H3K27me3. In contrast, myocardial cells located on the outer ventricular surface generally retained high H3K27me3 signal. By 5 dpf, trabecular cardiomyocyte H3K27me3 levels were largely normalized with those of the outer cardiomyocyte layer. However, Kdm6b is not uniquely responsible for the bulk transient H3K27me3 decrease associated with trabeculating cardiomyocytes in 3 dpf *kdm6b*-deficient larvae (Fig. S5). Instead, Kdm6b likely mediates myocardial cell cycle entry by promoting expression of a restricted set of target genes.

4. Discussion

Our investigation of histone demethylases *kdm6ba* and *kdm6bb* during zebrafish development presents several insights. First, we show how duplicated orthologous genes with retained overlapping expression can obscure loss-of-function phenotypes due to simple non-compensatory genetic redundancy. Second, we show that Kdm6b-family demethylases have pleiotropic roles during larval organ development rather than during embryonic cell specification or the establishment of initial organ "frameworks." Third, Kdm6b demethylases specifically contribute to cardiogenesis by supporting augmented cellular proliferation associated with the initiation of ventricular trabeculation during larval metamorphosis. Fourth, while developing heart ventricle cells display strikingly variable cellular H3K27me3 levels including a transient decrease in trabeculating cardiomyocytes, these bulk dynamics are not driven by Kdm6b proteins alone.

4.1. Kdm6b reverse genetic studies provide an example of straightforward non-compensatory redundancy between duplicated genes

Our combined genetic analysis of *kdm6bb* and *kdm6ba* illustrates how redundant functions between ohnologous genes can obscure the effects of single gene mutation without involving a compensatory network. As such, our study exemplifies how the lack of phenotypes frequently observed in homozygous mutant zebrafish can be attributed to buffering redundancy originating from the ancestral teleost whole genome duplication event (Amores, 1998; Postlethwait et al., 1998; Lawson, 2016). We suggest that straightforward non-compensatory redundancy be thoroughly considered during reverse genetic studies of ohnologous gene pairs, especially when expression patterns largely overlap.

4.2. Histone demethylases kdm6ba and kdm6bb share likely conserved roles in vertebrate organ maturation

Independently generated *Kdm6b* presumptive null alleles in mice are either pre-implantation (Ohtani et al., 2013) or perinatal (Burgold et al., 2012; Q. Li et al., 2014; Satoh et al., 2010; Shpargel et al., 2014; Zhang et al., 2015) lethal. Our zebrafish studies are consistent with the latter publications by suggesting that Kdm6b proteins primarily contribute to organ maturation rather than early cell fate specification, in contrast to some predictions (Kartikasari et al., 2013; Ohtani et al., 2011). These roles are likely evolutionarily conserved as the pleiotropic defects we observe in *kdm6b*-deficient zebrafish are reminiscent of those reported in mice. For example, *kdm6ba*$^{-/-}$; *kdm6bb*$^{-/-}$ fish display stunted craniofacial cartilage formation and *Kdm6b*-deficient mice develop skeletal dwarfism during early stages of bone development (Zhang et al., 2015). However, further experiments are necessary to determine if Kdm6b proteins have restricted roles in certain skeletal structures (e.g. the notably truncated basihyal cartilage in *kdm6b* double mutant zebrafish) or widely contribute to bone formation, as seen in mice. Similarly, the swim bladder defects we observed in our *kdm6b*-deficient zebrafish may parallel lung structure and respiration defects in *Kdm6b*-null mice (Q. Li et al., 2014b; Satoh et al., 2010) given the evolutionary homology between the teleost swim bladder and lungs of terrestrial vertebrates (Perry et al., 2001; Winata et al., 2009).

kdm6b-deficient zebrafish complete the initial stages of cardiac development, forming discrete heart chambers, an outflow tract, and valves. As such, earlier events including the generation and expansion of cardiac progenitors, specification and differentiation of endocardial and myocardial cells, and initial heart tube extension and looping do not require Kdm6b. This conclusion controverts reported roles of *Kdm6b* in mesodermal and cardiovascular differentiation derived from embryonic stem cell studies (Ohtani et al., 2011). However, our zebrafish studies are consistent with the preponderance of *Kdm6b* loss-of-function mouse models that survive to late fetal stages, indicating that overt cardiogenesis is substantially Kdm6b independent.

Although our study shows that combined *kdm6ba* and *kdm6bb* are not required for early embryonic development, they may have roles masked by further redundancy with *kdm6a* (*Utx*) genes. Mouse genetic studies show that *Kdm6a* has unique essential developmental functions, including in mesoderm lineage differentiation and cardiogenesis (Lee et al., 2012; Shpargel et al., 2012; Wang et al., 2012; Welstead et al., 2012). In contrast, *Kdm6b* and *Kdm6a* are proposed to function redundantly during murine thymocyte differentiation (Manna et al., 2015). Mechanistically, both Kdm6a and Kdm6b interact with the Brg1-associated factor chromatin remodeling complex (Miller et al., 2010). Conflicting reports also indicate that both Kdm6a and Kdm6b proteins may be components of MLL/COMPASS-like H3K4 methyltransferase complexes (De Santa et al., 2007; Issaeva et al., 2007; Williams et al., 2014). Collectively, these studies suggest Kdm6a and Kdm6b share a limited redundancy that is context dependent. The zebrafish genome contains two *Kdm6a* orthologs, *kdm6a*

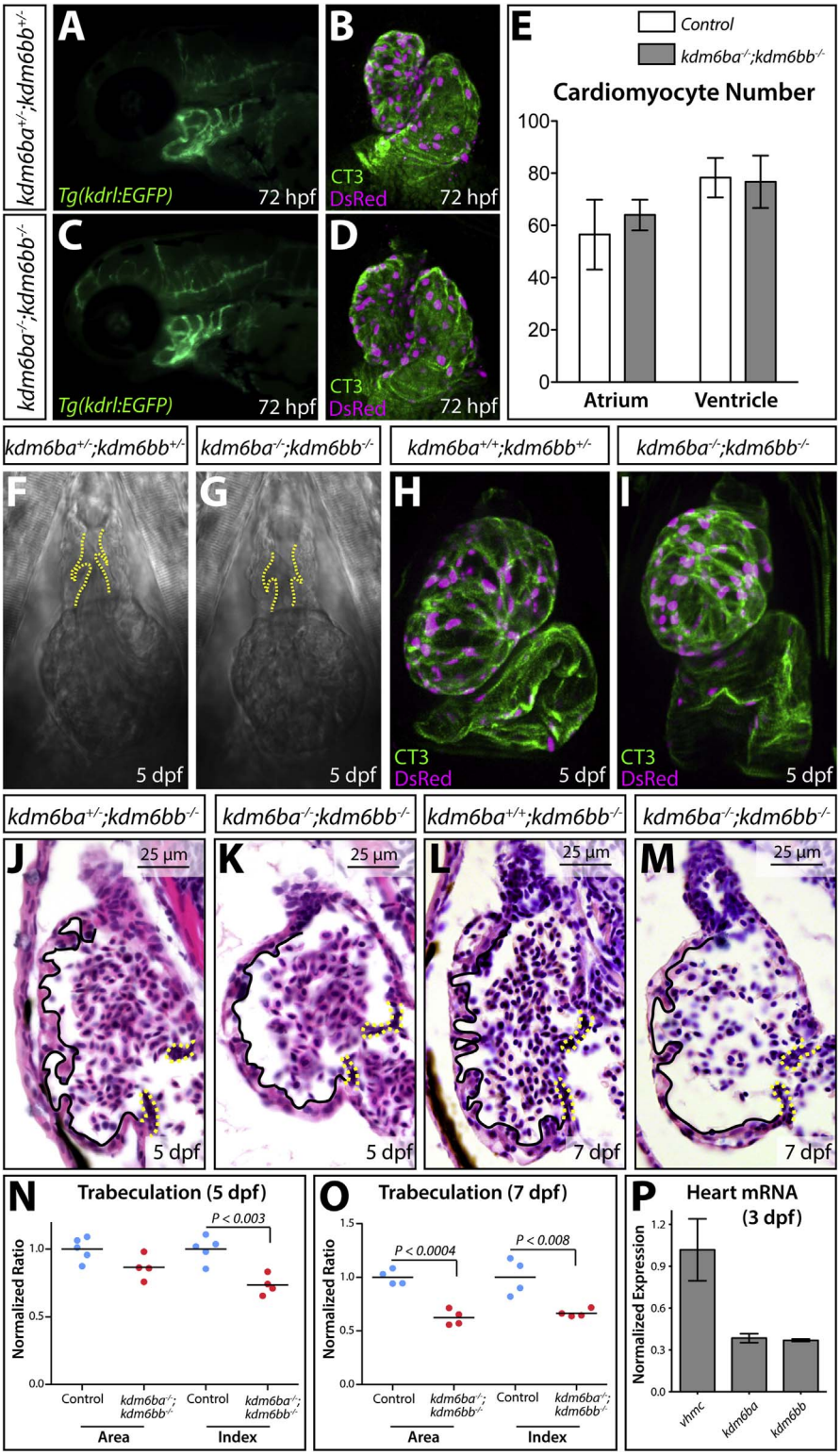

Fig. 4. *Kdm6ba* and *kdm6bb* redundantly promote cardiac trabeculation. (A, C) Fluorescent imaged whole mount 72 hpf embryos showing the aortic arch arteries of control and *kdm6b*-deficient *Tg(kdrl:EGFP)* animals. (B, D) Confocal heart images of whole mount 72 hpf *Tg(myl7:DsRed-nuc)* larvae antibody stained for DsRed (red, cardiomyocyte nuclei) and cardiac troponin (CT3, heart muscle). Control and combined *kdm6ba/kdm6bb*-deficient larvae are shown. (E) Bar graphs comparing the absolute number of atrial and ventricular cardiomyocytes between 72 hpf control (*kdm6ba*$^{+/-}$; *kdm6bb*$^{+/-}$ and *kdm6ba*$^{+/+}$; *kdm6bb*$^{+/-}$) and *kdm6ba*$^{-/-}$; *kdm6bb*$^{-/-}$ larvae. Error bars represent one standard deviation (n=6 control and 7 *kdm6ba/bb*-deficient fish from two clutches). (F, G) DIC microscopy images showing the OFT and ventricle of control and *kdm6b*-deficient embryos at 5 dpf. Dashed yellow lines outline the OFT valves. (H, I) Whole mount confocal imaged hearts of immunostained 5 dpf control and *kdm6ba*$^{-/-}$; *kdm6bb*$^{-/-}$ larvae. These *Tg(myl7:DsRed-nuc)* fish are stained with anti-DsRed (red, cardiomyocyte nuclei) and anti-cardiac troponin (CT3, green) antibodies. (J-M) H & E stained sagittal sections through the heart of 5 and 7 dpf control and *kdm6ba*$^{-/-}$; *kdm6bb*$^{-/-}$ larvae. Solid lines outline the trabeculae and dashed yellow lines indicate the AVC valves. (N, O) Scatterplot graphs showing the normalized outer curvature ventricular sectional area and trabeculation extent ("index") of 5 and 7 dpf control compared to clutch mate *kdm6ba*$^{-/-}$; *kdm6bb*$^{-/-}$ larvae. Each data point represents one animal. P-values are from Student's two-tailed *t*-tests. (P) Bar graph of qRT-PCR data comparing *kdm6ba* and *kdm6bb* to *vmhcl* transcript levels using three pools of isolated 3 dpf zebrafish embryonic hearts (normalized to *vmhcl* levels). Error bars are one standard deviation.

and *kdm6al*. While neither gene has been explored genetically, morpholino studies implicate both *kdm6a* and *kdm6al* in Hox-dependent body plan patterning, craniofacial cartilage development, heart looping, and brain morphology (Lan et al., 2007; Van Laarhoven et al., 2015). However, given concerns about morpholino specificity, reverse genetic studies examining *kdm6a* and *kdm6al* individually, together, and combined with our *kdm6b* alleles are necessary to validate and extend these studies.

4.3. Dynamic bulk H3K27me3 levels during cardiogenesis support a non-specific mode for H3K27me3 demethylases in enabling cell transitions

Zebrafish embryo genome-wide H3K27me3 and H3K4me3 studies show both marks are established at or prior to zygotic gene activation (3.3 hpf) and can co-localize at key regulatory genes (Lindeman et al., 2011; Vastenhouw et al., 2010). These observations support the ES-cell inspired model that targeted removal of H3K27me3 marks supports activation of epigenetically "poised" lineage-defining regulatory genes. In contrast, our *kdm6b* genetic studies are consistent with an opposing view that this bivalency model incompletely represents in vivo H3K4me3/H3K27me3 observations and the effects of disrupting either PRC2 or MLL/COMPASS activity (reviewed in Piunti and Shilatifard (2016)). In further support, genetic loss of combined maternal and zygotic *ezh2* and, resultantly, all H3K27me3 does not disrupt gastrulation or overall body plan establishment in zebrafish (San et al., 2016). Nevertheless, *ezh2*-null fish do show pleiotropic embryonic defects, including in heart development, that are consistent with widespread poorly maintained cell identities (San et al., 2016).

Bulk H3K27me3 levels are initially high in all ventricular cardiomyocytes, become notably depleted upon the initiation of cardiac trabeculation, and are then rapidly restored during ventricle maturation. These observed bulk H3K27me3 dynamics may reflect a large scale "re-programming" of the overall cellular H3K27me3 load that enables signaling effectors to promote a major cell transition at the onset of trabeculation. A conceptually similar but opposite process may occur during initial cardiac differentiation, as bulk H3K27me3 levels

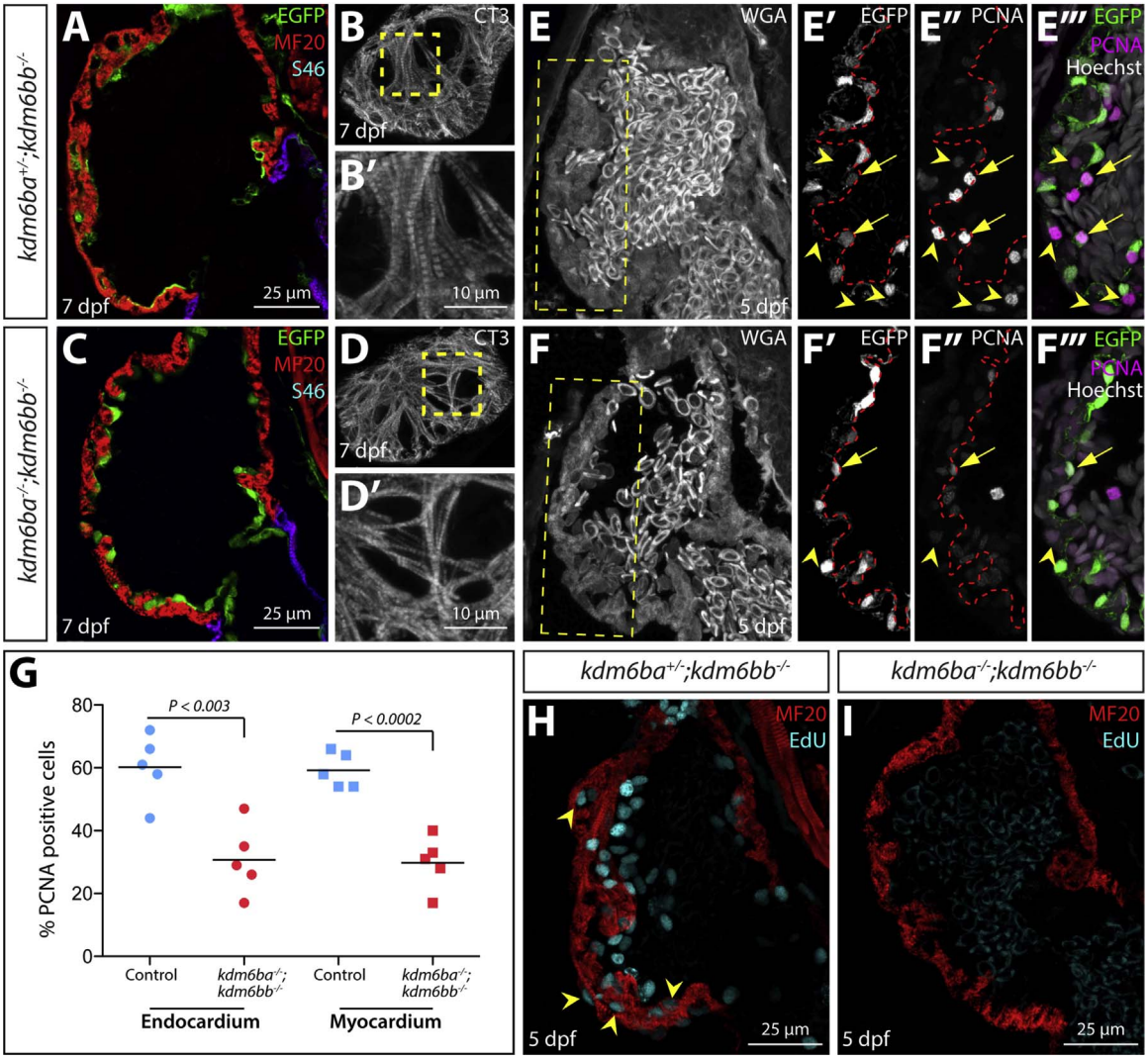

Fig. 5. Kdm6b proteins enable coordinated endocardial and myocardial proliferation associated with early stage ventricle maturation. (A-C) Confocal immunofluorescence images of sagittal heart sections from 5 dpf *kdm6b*- and *kdm6a*/*kdm6b*-deficient *Tg(kdrl:EGFP)* larvae stained with anti-GFP (green, endocardium), anti-myosin heavy chain (MF20, red, myocardium), and anti-S46 (magenta, atrial muscle) antibodies. (B, D) Cardiac troponin (CT3) antibody staining of superficial sections through the heart of 5 dpf *kdm6bb*$^{-/-}$ and *kdm6ba*$^{-/-}$; *kdm6bb*$^{-/-}$ larvae. B' and D' are zoomed images of the dashed yellow box regions. (E-F) Confocal imaged sagittal sections of 5 dpf control and combined *kdm6b*-deficient *Tg(kdrl:EGFP)* embryos stained with wheat germ agglutinin (WGA, grey) as well as anti-GFP (green in overlay panels, endocardium) and anti-PCNA (magenta in overlay panels) antibodies. Yellow boxes in E and F indicate zoomed regions shown in E'-F'''. Arrows and arrowheads mark PCNA-positive endocardial and myocardial cells, respectively. (G) Scatterplot graphs showing the number of PCNA positive endocardial and myocardial cells within the outer curvature ventricular wall scored from matched sagittal heart sections of 5 dpf control and *kdm6ba*$^{-/-}$; *kdm6bb*$^{-/-}$ larvae. Each point represents a distinct fish. P-values are from two-tailed Student's *t*-tests. (H, I) Confocal heart images of sagittal sectioned 5 dpf control and *kdm6a*/*kdm6b*-deficient larvae stained for EdU incorporation (cyan, proliferating cells) and with anti-myosin heavy chain antibody (red, MF20, cardiomyocytes).

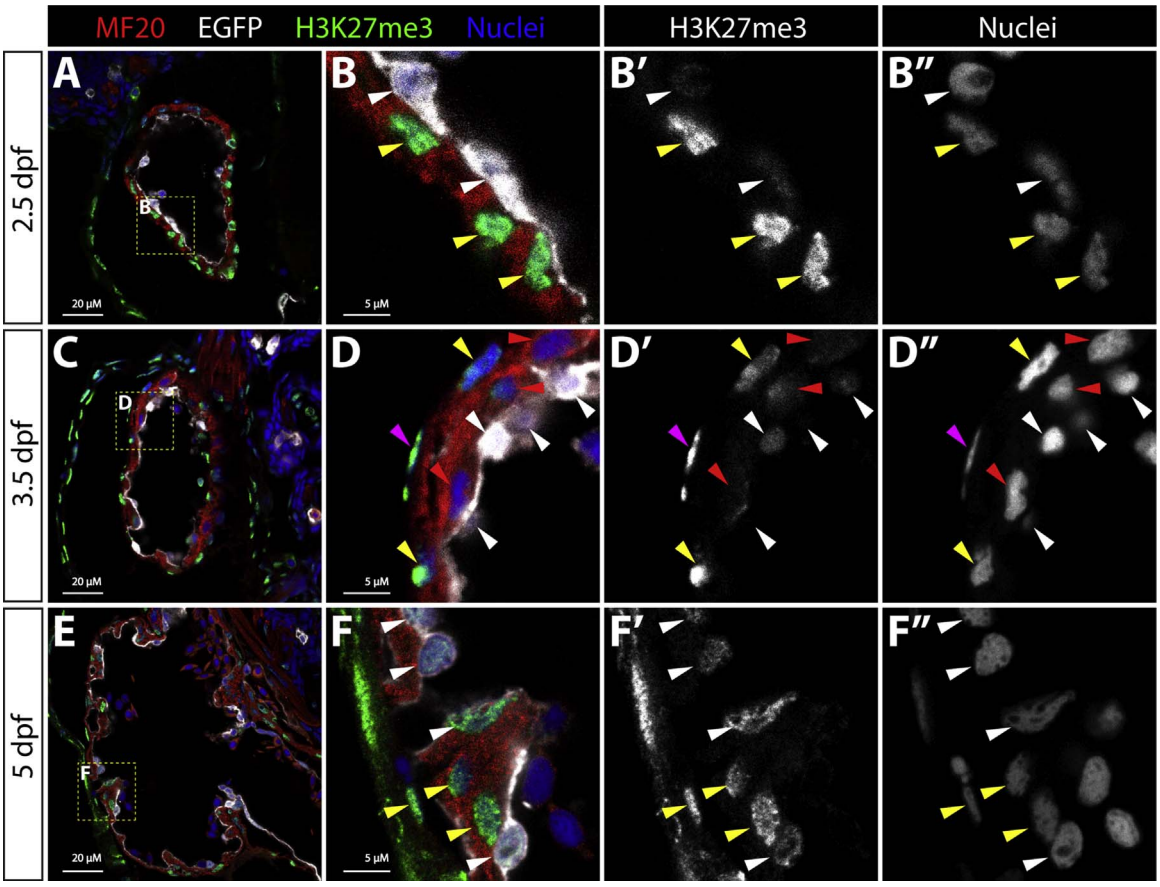

Fig. 6. Bulk cellular H3K27me3 levels transiently decrease in trabeculating cardiomyocytes. (A-F) Confocal microscopy immunofluorescence images of sagittal sections through the heart of 2.5, 3.5, and 5 dpf *Tg(kdrl:EGFP)* embryos stained with anti-myosin heavy chain (red, MF20, myocardium), anti-EGFP (white, endocardium), and anti-H3K27me3 (green) antibodies. Hoechst-stained nuclei are blue. Zoomed images of the yellow boxed areas (in A, C, and E) are shown in (B, D, and F) with adjacent single channel H3K27me3 and nuclei staining to highlight differences in bulk H3K27me3 levels. Magenta and white arrowheads indicate nuclei of epicardial and endocardial cells, respectively. Yellow and red arrowheads mark H3K27me3-high and H3K27me3-low cardiomyocyte nuclei, respectively. 20 μM and 5 μM (zoom panels) scale bars are shown.

rapidly increase as progenitor-like second heart field cells initiate differentiation while appending to the cardiac poles (Delgado-Olguín et al., 2012).

Extending this paradigm, the epigenetic "de-silencing" of repressed genes sometimes may occur by the "bulk" demethylation of H3K27me3-marked nucleosomes rather than by the local action of demethylases on specific subsets of silenced regulatory regions. The specificity of transcriptional responses then is driven by transcription factors acting largely independently from "passively" enabling histone demethylases. This concept supports the re-emerging idea that PRC2-catalyzed H3K27me3 marks maintain rather than specify a transcriptionally repressed state (Comet et al., 2016), as indicated by original *Drosophila* Polycomb/Trithorax studies. By extension, bulk removal of H3K27me3 marks, as we observed during cardiogenesis, may occur only in specialized developmental, homeostatic, or repair instances. Such roles potentially would enable, but not instruct, major cell state reversals (e.g. de-differentiation, epithelial-to-mesenchymal transitions, or cell cycle re-entry).

4.4. Histone demethylases kdm6ba and kdm6bb promote proliferation coupled with the initiation of cardiac trabeculation

Trabeculation of the zebrafish ventricle initiates around 72 hpf with the specification of a small number of trabeculating cardiomyocytes that separate from the otherwise single cell-thick outer myocardial layer (Gupta and Poss, 2012; Han et al., 2016; Liu et al., 2010; Peshkovsky et al., 2011). These specialized trabeculating cardiomyocytes then clonally expand during early larval stages to form extensive ridge-like cardiac trabeculae that protrude into the ventricular cavity. The initial phase of trabeculation driven by neuregulin/ErbB2 signaling (Han et al., 2016; Liu et al., 2010; Peshkovsky et al., 2011) does not depend on Kdm6b as we saw that small groups of multiple cell layer thick myocardium still form in *kdm6b*-deficient fish. Instead, Kdm6b is required for the subsequent boost of proliferation at larval hatching (around 96 hpf) seen in trabeculating myocardial cells (Gupta and Poss, 2012; Han et al., 2016; Liu et al., 2010) as well as adjacent endocardium that concomitantly expands to enshroud the forming trabeculae.

Kdm6b alone appears unlikely to drive the bulk H3K27me3 demethylation in trabeculating cardiomyocytes. Instead, Kdm6b could provide an "epigenetic" component to transcriptional switches acting on a discrete set of target genes by locally removing H3K27me3 marks or, by a non-catalytic role as part of a MLL/COMPASS H3K4 methylase complex. Of potential relevance, the Kdm6b-cooperating Brg1-associated factor (BAF) chromatin remodeling complex (Miller et al., 2010) enables trabeculation in mice by repressing endocardial transcription of the trabeculation-suppressing Adamts1 matrix protease (Stankunas et al., 2008). Another possibility is that Kdm6b acts in both myocardial and endocardial cells to integrate a systemic signal that widely coordinates organ maturation events coupled to larval metamorphosis. Thyroid hormone is one immediate candidate that is upregulated upon hatching (Chang et al., 2012) and a suspected cardiomyocyte mitogen in mammals (Ledda-Columbano et al., 2006; M. Li et al., 2014; Naqvi et al., 2014). Regardless, the role of Kdm6b in promoting cardiomyocyte proliferation establishes these histone demethylases and downstream target genes as candidate genes for congenital heart defects of

the ventricle such as hypoplastic left ventricle syndrome.

The recognition that differentiated cardiomyocytes can re-acquire robust proliferative ability during heart regeneration in both zebrafish and mice (Jopling et al., 2010; Porrello et al., 2011; Poss et al., 2002) and that mammalian cardiomyocytes may retain some proliferative capacity during pre-adolescence (Ali et al., 2014; Haubner et al., 2016; Mollova et al., 2013; Naqvi et al., 2014; Polizzotti et al., 2015; Ye et al., 2016) has focused efforts to recapitulate these mechanisms to repair damaged heart muscle. The role of Kdm6b histone demethylases in developmentally timed cardiomyocyte (but not cardiac progenitor) proliferation suggests the reversal of epigenetic H3K27me3 silencing marks may be an essential aspect of innate heart regeneration and a promising path to augment therapeutically delivered cardiomyocytes for heart disease.

Author contributions

A.A.A. designed and performed most of the experiments and wrote the manuscript. A.H. performed experiments and assisted with figure preparation. S.S. and K.S. designed and performed experiments and wrote the manuscript.

Funding sources

A.A.A. received support from a NIH/NICHD Developmental Biology Training Grant (5T32HD007348). Research funding was provided by the University of Oregon and the National Institutes of Health (1R01HL115294, K.S.).

Acknowledgements

We thank the University of Oregon zebrafish facility and staff. The Stankunas lab and the University of Oregon zebrafish community provided critical guidance and support. Caroline and Geoffrey Burns shared qRT-PCR primers for *rps11* and *vmhcl* and provided technical advice. Jamie Nichols and Chuck Kimmel shared insights about and protocols for studying craniofacial development. Judith Eisen provided critical feedback on the manuscript.

Appendix A. Supporting information

Supplementary data associated with this article can be found in the online version at doi:10.1016/j.ydbio.2017.03.030.

References

Akerberg, A.A., Stewart, S., Stankunas, K., 2014. Spatial and temporal control of transgene expression in zebrafish. PLoS One 9, e92217. http://dx.doi.org/10.1371/journal.pone.0092217.

Akerberg, B.N., Sarangam, M.L., Stankunas, K., 2015. Endocardial Brg1 disruption illustrates the developmental origins of semilunar valve disease. Dev. Biol. 407, 158–172. http://dx.doi.org/10.1016/j.ydbio.2015.06.015.

Alder, O., Lavial, F., Helness, A., Brookes, E., Pinho, S., Chandrashekran, A., Arnaud, P., Pombo, A., O'Neill, L., Azuara, V., 2010. Ring1B and Suv39h1 delineate distinct chromatin states at bivalent genes during early mouse lineage commitment. Development 137, 2483–2492. http://dx.doi.org/10.1242/dev.048363.

Ali, S.R., Hippenmeyer, S., Saadat, L.V., Luo, L., Weissman, I.L., Ardehali, R., 2014. Existing cardiomyocytes generate cardiomyocytes at a low rate after birth in mice. Proc. Natl. Acad. Sci. USA 111, 8850–8855. http://dx.doi.org/10.1073/pnas.1408233111.

Amores, A., 1998. Zebrafish hox clusters and vertebrate genome evolution. Science 282, 1711–1714. http://dx.doi.org/10.1126/science.282.5394.1711.

Azuara, V., Perry, P., Sauer, S., Spivakov, M., Jørgensen, H.F., John, R.M., Gouti, M., Casanova, M., Warnes, G., Merkenschlager, M., Fisher, A.G., 2006. Chromatin signatures of pluripotent cell lines. Nat. Cell Biol. 8, 532–538. http://dx.doi.org/10.1038/ncb1403.

Bassett, A.R., Tibbit, C., Ponting, C.P., Liu, J.-L., 2013. Highly efficient targeted mutagenesis of Drosophila with the CRISPR/Cas9 system. Cell Rep. 4, 220–228. http://dx.doi.org/10.1016/j.celrep.2013.06.020.

Bernstein, B.E., Mikkelsen, T.S., Xie, X., Kamal, M., Huebert, D.J., Cuff, J., Fry, B., Meissner, A., Wernig, M., Plath, K., Jaenisch, R., Wagschal, A., Feil, R., Schreiber, S.L., Lander, E.S., 2006. A bivalent chromatin structure marks key developmental genes in embryonic stem cells. Cell 125, 315–326. http://dx.doi.org/10.1016/j.cell.2006.02.041.

Burgold, T., Spreafico, F., De Santa, F., Totaro, M.G., Prosperini, E., Natoli, G., Testa, G., 2008. The histone H3 lysine 27-specific demethylase Jmjd3 is required for neural commitment. PLoS One 3, e3034. http://dx.doi.org/10.1371/journal.pone.0003034.

Burgold, T., Voituron, N., Caganova, M., Tripathi, P.P., Menuet, C., Tusi, B.K., Spreafico, F., Bévengut, M., Gestreau, C., Buontempo, S., Simeone, A., Kruidenier, L., Natoli, G., Casola, S., Hilaire, G., Testa, G., 2012. The H3K27 demethylase JMJD3 is required for maintenance of the embryonic respiratory neuronal network, neonatal breathing, and survival. Cell Rep. 2, 1244–1258. http://dx.doi.org/10.1016/j.celrep.2012.09.013.

Cao, R., Wang, L., Wang, H., Xia, L., Erdjument-Bromage, H., Tempst, P., Jones, R.S., Zhang, Y., 2002. Role of histone H3 lysine 27 methylation in polycomb-group silencing. Science 298, 1039–1043. http://dx.doi.org/10.1126/science.1076997.

Chang, J., Wang, M., Gui, W., Zhao, Y., Yu, L., Zhu, G., 2012. Changes in thyroid hormone levels during zebrafish development. Zool. Sci. 29, 181–184. http://dx.doi.org/10.2108/zsj.29.181.

Cloos, P.A.C., Christensen, J., Agger, K., Helin, K., 2008. Erasing the methyl mark: histone demethylases at the center of cellular differentiation and disease. Genes Dev. 22, 1115–1140. http://dx.doi.org/10.1101/gad.1652908.

Comet, I., Riising, E.M., Leblanc, B., Helin, K., 2016. Maintaining cell identity: PRC2-mediated regulation of transcription and cancer. Nat. Rev. Cancer 16, 803–810. http://dx.doi.org/10.1038/nrc.2016.83.

Dahl, J.A., Reiner, A.H., Klungland, A., Wakayama, T., Collas, P., 2010. Histone H3 lysine 27 methylation asymmetry on developmentally-regulated promoters distinguish the first two lineages in mouse preimplantation embryos. PLoS One 5, e9150. http://dx.doi.org/10.1371/journal.pone.0009150.

De Santa, F., Totaro, M.G., Prosperini, E., Notarbartolo, S., Testa, G., Natoli, G., 2007. The histone H3 lysine-27 demethylase Jmjd3 links inflammation to inhibition of polycomb-mediated gene silencing. Cell 130, 1083–1094. http://dx.doi.org/10.1016/j.cell.2007.08.019.

Delgado-Olguín, P., Huang, Y., Li, X., Christodoulou, D., Seidman, C.E., Seidman, J.G., Tarakhovsky, A., Bruneau, B.G., 2012. Epigenetic repression of cardiac progenitor gene expression by Ezh2 is required for postnatal cardiac homeostasis. Nat. Genet. 44, 343–347. http://dx.doi.org/10.1038/ng.1068.

Force, A., Lynch, M., Pickett, F.B., Amores, A., Yan, Y.L., Postlethwait, J., 1999. Preservation of duplicate genes by complementary, degenerative mutations. Genetics 151, 1531–1545.

Gupta, V., Poss, K.D., 2012. Clonally dominant cardiomyocytes direct heart morphogenesis. Nature 484, 479–484. http://dx.doi.org/10.1038/nature11045.

Han, P., Bloomekatz, J., Ren, J., Zhang, R., Grinstein, J.D., Zhao, L., Burns, C.G., Burns, C.E., Anderson, R.M., Chi, N.C., 2016. Coordinating cardiomyocyte interactions to direct ventricular chamber morphogenesis. Nature 534, 700–704. http://dx.doi.org/10.1038/nature18310.

Haubner, B.J., Schneider, J., Schweigmann, U., 2016. Functional recovery of a human neonatal heart after severe myocardial infarction. Circulation 118, 216–221. http://dx.doi.org/10.1161/CIRCRESAHA.116.307017.

He, A., Ma, Q., Cao, J., Gise, von, A., Zhou, P., Xie, H., Zhang, B., Hsing, M., Christodoulou, D.C., Cahan, P., Daley, G.Q., Kong, S.W., Orkin, S.H., Seidman, C.E., Seidman, J.G., Pu, W.T., 2012. Polycomb repressive complex 2 regulates normal development of the mouse heart. Circ. Res. 110, 406–415. http://dx.doi.org/10.1161/CIRCRESAHA.111.252205.

Hong, S., Cho, Y.-W., Yu, L.-R., Yu, H., Veenstra, T.D., Ge, K., 2007. Identification of JmjC domain-containing UTX and JMJD3 as histone H3 lysine 27 demethylases. Proc. Natl. Acad. Sci. USA 104, 18439–18444. http://dx.doi.org/10.1073/pnas.0707292104.

Issaeva, I., Zonis, Y., Rozovskaia, T., Orlovsky, K., Croce, C.M., Nakamura, T., Mazo, A., Eisenbach, L., Canaani, E., 2007. Knockdown of ALR (MLL2) reveals ALR target genes and leads to alterations in cell adhesion and growth. Mol. Cell. Biol. 27, 1889–1903. http://dx.doi.org/10.1128/MCB.01506-06.

Jaillon, O., Aury, J.-M., Brunet, F., Petit, J.-L., Stange-Thomann, N., Mauceli, E., Bouneau, L., Fischer, C., Ozouf-Costaz, C., Bernot, A., Nicaud, S., Jaffe, D., Fisher, S., Lutfalla, G., Dossat, C., Segurens, B., Dasilva, C., Salanoubat, M., Levy, M., Boudet, N., Castellano, S., Anthouard, V., Jubin, C., Castelli, V., Katinka, M., Vacherie, B., Biémont, C., Skalli, Z., Cattolico, L., Poulain, J., De Berardinis, V., Cruaud, C., Duprat, S., Brottier, P., Coutanceau, J.-P., Gouzy, J., Parra, G., Lardier, G., Chapple, C., McKernan, K.J., McEwan, P., Bosak, S., Kellis, M., Volff, J.-N., Guigó, R., Zody, M.C., Mesirov, J., Lindblad-Toh, K., Birren, B., Nusbaum, C., Kahn, D., Robinson-Rechavi, M., Laudet, V., Schachter, V., Quétier, F., Saurin, W., Scarpelli, C., Wincker, P., Lander, E.S., Weissenbach, J., Roest Crollius, H., 2004. Genome duplication in the teleost fish Tetraodon nigroviridis reveals the early vertebrate proto-karyotype. Nature 431, 946–957. http://dx.doi.org/10.1038/nature03025.

Jao, L.-E., Wente, S.R., Chen, W., 2013. Efficient multiplex biallelic zebrafish genome editing using a CRISPR nuclease system. Proc. Natl. Acad. Sci. USA 110, 13904–13909. http://dx.doi.org/10.1073/pnas.1308335110.

Jiang, W., Wang, J., Zhang, Y., 2013. Histone H3K27me3 demethylases KDM6A and KDM6B modulate definitive endoderm differentiation from human ESCs by regulating WNT signaling pathway. Cell Res. 23, 122–130. http://dx.doi.org/10.1038/cr.2012.119.

Jin, S.-W., Beis, D., Mitchell, T., Chen, J.-N., Stainier, D.Y.R., 2005. Cellular and molecular analyses of vascular tube and lumen formation in zebrafish. Development 132, 5199–5209. http://dx.doi.org/10.1242/dev.02087.

Jopling, C., Sleep, E., Raya, M., Martí, M., Raya, A., Izpisua Belmonte, J.C., 2010. Zebrafish heart regeneration occurs by cardiomyocyte dedifferentiation and proliferation. Nature 464, 606–609. http://dx.doi.org/10.1038/nature08899.

Kartikasari, A.E.R., Zhou, J.X., Kanji, M.S., Chan, D.N., Sinha, A., Grapin-Botton, A., Magnuson, M.A., Lowry, W.E., Bhushan, A., 2013. The histone demethylase Jmjd3 sequentially associates with the transcription factors Tbx3 and Eomes to drive endoderm differentiation. EMBO J. 32, 1393–1408. http://dx.doi.org/10.1038/emboj.2013.78.

Klose, R.J., Zhang, Y., 2007. Regulation of histone methylation by demethylimination and demethylation. Nat. Rev. Mol. Cell Biol. 8, 307–318. http://dx.doi.org/10.1038/nrm2143.

Lan, F., Bayliss, P.E., Rinn, J.L., Whetstine, J.R., Wang, J.K., Chen, S., Iwase, S., Alpatov, R., Issaeva, I., Canaani, E., Roberts, T.M., Chang, H.Y., Shi, Y., 2007. A histone H3 lysine 27 demethylase regulates animal posterior development. Nature 449, 689–694. http://dx.doi.org/10.1038/nature06192.

Lawson, N.D., 2016. Reverse genetics in zebrafish: mutants, morphants, and moving forward. Trends Cell Biol. 26, 77–79. http://dx.doi.org/10.1016/j.tcb.2015.11.005.

Ledda-Columbano, G.M., Molotzu, F., Pibiri, M., Cossu, C., Perra, A., Columbano, A., 2006. Thyroid hormone induces cyclin D1 nuclear translocation and DNA synthesis in adult rat cardiomyocytes. FASEB J. 20, 87–94. http://dx.doi.org/10.1096/fj.05-4202com.

Lee, S., Lee, J.W., Lee, S.-K., 2012. UTX, a histone H3-lysine 27 demethylase, acts as a critical switch to activate the cardiac developmental program. Dev. Cell 22, 25–37. http://dx.doi.org/10.1016/j.devcel.2011.11.009.

Li, M., Iismaa, S.E., Naqvi, N., Nicks, A., Husain, A., Graham, R.M., 2014a. Thyroid hormone action in postnatal heart development. Stem Cell Res. 13, 582–591. http://dx.doi.org/10.1016/j.scr.2014.07.001.

Li, Q., Wang, H.Y., Chepelev, I., Zhu, Q., Wei, G., Zhao, K., Wang, R.-F., 2014b. Stage-dependent and locus-specific role of histone demethylase Jumonji D3 (JMJD3) in the embryonic stages of lung development. PLoS Genet. 10, e1004524. http://dx.doi.org/10.1371/journal.pgen.1004524.s011.

Lindeman, L.C., Andersen, I.S., Reiner, A.H., Li, N., Aanes, H., Østrup, O., Winata, C., Mathavan, S., Müller, F., Aleström, P., Collas, P., 2011. Prepatterning of developmental gene expression by modified histones before zygotic genome activation. Dev. Cell 21, 993–1004. http://dx.doi.org/10.1016/j.devcel.2011.10.008.

Liu, J., Bressan, M., Hassel, D., Huisken, J., Staudt, D., Kikuchi, K., Poss, K.D., Mikawa, T., Stainier, D.Y.R., 2010. A dual role for ErbB2 signaling in cardiac trabeculation. Development 154, 459–473. http://dx.doi.org/10.1242/dev.053736.

Lynch, M., Force, A., 2000. A dual role for ErbB2 signaling in cardiac trabeculation. Development 137, 3867–3875.

Manna, S., Kim, J.K., Baugé, C., Cam, M., Zhao, Y., Shetty, J., Vacchio, M.S., Castro, E., Tran, B., Tessarollo, L., Bosselut, R., 2015. Histone H3 Lysine 27 demethylases Jmjd3 and Utx are required for T-cell differentiation. Nat. Commun. 6, 8152. http://dx.doi.org/10.1038/ncomms9152.

Margueron, R., Reinberg, D., 2011. The Polycomb complex PRC2 and its mark in life. Nature 469, 343–349. http://dx.doi.org/10.1038/nature09784.

Meyer, A., Schartl, M., 1999. Gene and genome duplications in vertebrates: the one-to-four (-to-eight in fish) rule and the evolution of novel gene functions. Curr. Opin. Cell Biol. 11, 699–704. http://dx.doi.org/10.1016/S0955-0674(99)00039-3.

Mikkelsen, T.S., Ku, M., Jaffe, D.B., Issac, B., Lieberman, E., Giannoukos, G., Alvarez, P., Brockman, W., Kim, T.-K., Koche, R.P., Lee, W., Mendenhall, E., O'Donovan, A., Presser, A., Russ, C., Xie, X., Meissner, A., Wernig, M., Jaenisch, R., Nusbaum, C., Lander, E.S., Bernstein, B.E., 2007. Genome-wide maps of chromatin state in pluripotent and lineage-committed cells. Nature 448, 553–560. http://dx.doi.org/10.1038/nature06008.

Miller, S.A., Mohn, S.E., Weinmann, A.S., 2010. Jmjd3 and UTX play a demethylase-independent role in chromatin remodeling to regulate T-box family member-dependent gene expression. Mol. Cell 40, 594–605. http://dx.doi.org/10.1016/j.molcel.2010.10.028.

Mollova, M., Bersell, K., Walsh, S., Savla, J., Das, L.T., Park, S.-Y., Silberstein, L.E., Remedios, Dos, C.G., Graham, D., Colan, S., Kühn, B., 2013. Cardiomyocyte proliferation contributes to heart growth in young humans. Proc. Natl. Acad. Sci. USA 110, 1446–1451. http://dx.doi.org/10.1073/pnas.1214608110.

Mosammaparast, N., Shi, Y., 2010. Reversal of histone methylation: biochemical and molecular mechanisms of histone demethylases. Annu. Rev. Biochem. 79, 155–179. http://dx.doi.org/10.1146/annurev.biochem.78.070907.103946.

Müller, J., Hart, C.M., Francis, N.J., Vargas, M.L., Sengupta, A., Wild, B., Miller, E.L., O'Connor, M.B., Kingston, R.E., Simon, J.A., 2002. Histone methyltransferase activity of a Drosophila Polycomb group repressor complex. Cell 111, 197–208. http://dx.doi.org/10.1016/S0092-8674(02)00976-5.

Naqvi, N., Li, M., Calvert, J.W., Tejada, T., Lambert, J.P., Wu, J., Kesteven, S.H., Holman, S.R., Matsuda, T., Lovelock, J.D., Howard, W.W., Iismaa, S.E., Chan, A.Y., Crawford, B.H., Wagner, M.B., Martin, D.I.K., Lefer, D.J., Graham, R.M., Husain, A., 2014. A proliferative burst during preadolescence establishes the final cardiomyocyte number. Cell 157, 795–807. http://dx.doi.org/10.1016/j.cell.2014.03.035.

Ohtani, K., Vlachojannis, G.J., Koyanagi, M., Boeckel, J.N., Urbich, C., Farcas, R., Bonig, H., Marquez, V.E., Zeiher, A.M., Dimmeler, S., 2011. Epigenetic regulation of endothelial lineage committed genes in pro-angiogenic hematopoietic and endothelial progenitor cells. Circ. Res. 109, 1219–1229. http://dx.doi.org/10.1161/CIRCRESAHA.111.247304.

Ohtani, K., Zhao, C., Dobreva, G., Manavski, Y., Kluge, B., Braun, T., Rieger, M.A., Zeiher, A.M., Dimmeler, S., 2013. Jmjd3 controls mesodermal and cardiovascular differentiation of embryonic stem cells. Circ. Res. 113, 856–862. http://dx.doi.org/10.1161/CIRCRESAHA.113.302035.

Paige, S.L., Thomas, S., Stoick-Cooper, C.L., Wang, H., Maves, L., Sandstrom, R., Pabon, L., Reinecke, H., Pratt, G., Keller, G., Moon, R.T., Stamatoyannopoulos, J., Murry, C.E., 2012. A temporal chromatin signature in human embryonic stem cells identifies regulators of cardiac development. Cell 151, 221–232. http://dx.doi.org/10.1016/j.cell.2012.08.027.

Perry, S.F., Wilson, R.J., Straus, C., Harris, M.B., Remmers, J.E., 2001. Which came first, the lung or the breath? Comp. Biochem. Physiol., Part A Mol. Integr. Physiol. 129, 37–47.

Peshkovsky, C., Totong, R., Yelon, D., 2011. Dependence of cardiac trabeculation on neuregulin signaling and blood flow in zebrafish. Dev. Dyn. 240, 446–456. http://dx.doi.org/10.1002/dvdy.22526.

Piunti, A., Shilatifard, A., 2016. Epigenetic balance of gene expression by Polycomb and COMPASS families. Science 352, aad9780. http://dx.doi.org/10.1126/science.aad9780.

Polizzotti, B.D., Ganapathy, B., Walsh, S., Choudhury, S., Ammanamanchi, N., Bennett, D.G., Remedios, Dos, C.G., Haubner, B.J., Penninger, J.M., Kühn, B., 2015. Neuregulin stimulation of cardiomyocyte regeneration in mice and human myocardium reveals a therapeutic window. Sci. Transl. Med. 7, 281ra45. http://dx.doi.org/10.1126/scitranslmed.aaa5171.

Porrello, E.R., Mahmoud, A.I., Simpson, E., Hill, J.A., Richardson, J.A., Olson, E.N., Sadek, H.A., 2011. Transient regenerative potential of the neonatal mouse heart. Science 331, 1078–1080. http://dx.doi.org/10.1126/science.1200708.

Poss, K.D., Wilson, L.G., Keating, M.T., 2002. Heart regeneration in zebrafish. Science 298, 2188–2190. http://dx.doi.org/10.1126/science.1077857.

Postlethwait, J.H., 2007. The zebrafish genome in context: ohnologs gone missing. J. Exp. Zool. B Mol. Dev. Evol. 308, 563–577. http://dx.doi.org/10.1002/jez.b.21137.

Postlethwait, J.H., Yan, Y.L., Gates, M.A., Horne, S., 1998. Vertebrate genome evolution and the zebrafish gene map. Nat. Genet. 18, 345–349. http://dx.doi.org/10.1038/ng0498-345.

Ramadoss, S., Chen, X., Wang, C.-Y., 2012. Histone demethylase KDM6B promotes epithelial-mesenchymal transition. J. Biol. Chem. 287, 44508–44517. http://dx.doi.org/10.1074/jbc.M112.424903.

Rugg-Gunn, P.J., Cox, B.J., Ralston, A., Rossant, J., 2010. Distinct histone modifications in stem cell lines and tissue lineages from the early mouse embryo. Proc. Natl. Acad. Sci. USA 107, 10783–10790. http://dx.doi.org/10.1073/pnas.0914507107.

San, B., Chrispijn, N.D., Wittkopp, N., van Heeringen, S.J., Lagendijk, A.K., Aben, M., Bakkers, J., Ketting, R.F., Kamminga, L.M., 2016. Normal formation of a vertebrate body plan and loss of tissue maintenance in the absence of ezh2. Sci. Rep. 6, 24658. http://dx.doi.org/10.1038/srep24658.

Satoh, T., Takeuchi, O., Vandenbon, A., Yasuda, K., Tanaka, Y., Kumagai, Y., Miyake, T., Matsushita, K., Okazaki, T., Saitoh, T., Honma, K., Matsuyama, T., Yui, K., Tsujimura, T., Standley, D.M., Nakanishi, K., Nakai, K., Akira, S., 2010. The Jmjd3-Irf4 axis regulates M2 macrophage polarization and host responses against helminth infection. Nat. Immunol. 11, 936–944. http://dx.doi.org/10.1038/ni.1920.

Shpargel, K.B., Sengoku, T., Yokoyama, S., Magnuson, T., 2012. UTX and UTY demonstrate histone demethylase-independent function in mouse embryonic development. PLoS Genet. 8, e1002964. http://dx.doi.org/10.1371/journal.pgen.1002964.t001.

Shpargel, K.B., Starmer, J., Yee, D., Pohlers, M., Magnuson, T., 2014. KDM6 demethylase independent loss of histone H3 Lysine 27 trimethylation during early embryonic development. PLoS Genet. 10, e1004507. http://dx.doi.org/10.1371/journal.pgen.1004507.s012.

Stankunas, K., Hang, C.T., Tsun, Z.-Y., Chen, H., Lee, N.V., Wu, J.I., Shang, C., Bayle, J.H., Shou, W., Iruela-Arispe, M.L., Chang, C.-P., 2008. Endocardial Brg1 represses ADAMTS1 to maintain the microenvironment for myocardial morphogenesis. Dev. Cell 14, 298–311. http://dx.doi.org/10.1016/j.devcel.2007.11.018.

Steinke, D., Salzburger, W., Braasch, I., Meyer, A., 2006. Many genes in fish have species-specific asymmetric rates of molecular evolution. BMC Genom. 7, 20. http://dx.doi.org/10.1186/1471-2164-7-20.

Stewart, S., Tsun, Z.-Y., Izpisua Belmonte, J.C., 2009. A histone demethylase is necessary for regeneration in zebrafish. Proc. Natl. Acad. Sci. USA 106, 19889–19894. http://dx.doi.org/10.1073/pnas.0904132106.

Takeuchi, J.K., Lou, X., Alexander, J.M., Sugizaki, H., Delgado-Olguín, P., Holloway, A.K., Mori, A.D., Wylie, J.N., Munson, C., Zhu, Y., Zhou, Y.-Q., Yeh, R.-F., Henkelman, R.M., Harvey, R.P., Metzger, D., Chambon, P., Stainier, D.Y.R., Pollard, K.S., Scott, I.C., Bruneau, B.G., 2011. Chromatin remodelling complex dosage modulates transcription factor function in heart development. Nat. Commun. 2, 187. http://dx.doi.org/10.1038/ncomms1187.

Thisse, C., Thisse, B., 2008. High-resolution in situ hybridization to whole-mount zebrafish embryos. Nat. Protoc. 3, 59–69. http://dx.doi.org/10.1038/nprot.2007.514.

Van Laarhoven, P.M., Neitzel, L.R., Quintana, A.M., Geiger, E.A., Zackai, E.H., Clouthier, D.E., Artinger, K.B., Ming, J.E., Shaikh, T.H., 2015. Kabuki syndrome genes KMT2D and KDM6A: functional analyses demonstrate critical roles in craniofacial, heart and brain development. Hum. Mol. Genet. 24, 4443–4453. http://dx.doi.org/10.1093/hmg/ddv180.

Vastenhouw, N.L., Zhang, Y., Woods, I.G., Imam, F., Regev, A., Liu, X.S., Rinn, J., Schier, A.F., 2010. Chromatin signature of embryonic pluripotency is established during genome activation. Nature 464, 922–926. http://dx.doi.org/10.1038/nature08866.

Walker, M.B., Kimmel, C.B., 2007. A two-color acid-free cartilage and bone stain for zebrafish larvae. Biotech. Histochem. 82, 23–28. http://dx.doi.org/10.1080/10520290701333558.

Wamstad, J.A., Alexander, J.M., Truty, R.M., Shrikumar, A., Li, F., Eilertson, K.E., Ding, H., Wylie, J.N., Pico, A.R., Capra, J.A., Erwin, G., Kattman, S.J., Keller, G.M., Srivastava, D., Levine, S.S., Pollard, K.S., Holloway, A.K., Boyer, L.A., Bruneau, B.G., 2012. Dynamic and coordinated epigenetic regulation of developmental transitions in the cardiac lineage. Cell 151, 206–220. http://dx.doi.org/10.1016/j.cell.2012.07.035.

Wang, C., Lee, J.-E., Cho, Y.-W., Xiao, Y., Jin, Q., Liu, C., Ge, K., 2012. UTX regulates mesoderm differentiation of embryonic stem cells independent of H3K27 demethylase activity. Proc. Natl. Acad. Sci. USA 109, 15324–15329. http://

dx.doi.org/10.1073/pnas.1204166109.
Welstead, G.G., Creyghton, M.P., Bilodeau, S., Cheng, A.W., Markoulaki, S., Young, R.A., Jaenisch, R., 2012. X-linked H3K27me3 demethylase Utx is required for embryonic development in a sex-specific manner. Proc. Natl. Acad. Sci. USA 109, 13004–13009. http://dx.doi.org/10.1073/pnas.1210787109.
Williams, K., Christensen, J., Rappsilber, J., Nielsen, A.L., Johansen, J.V., Helin, K., 2014. The histone lysine demethylase JMJD3/KDM6B is recruited to p53 bound promoters and enhancer elements in a p53 dependent manner. PLoS One 9, e96545. http://dx.doi.org/10.1371/journal.pone.0096545.
Winata, C.L., Korzh, S., Kondrychyn, I., Zheng, W., Korzh, V., Gong, Z., 2009. Development of zebrafish swimbladder: the requirement of Hedgehog signaling in specification and organization of the three tissue layers. Dev. Biol. 331, 222–236. http://dx.doi.org/10.1016/j.ydbio.2009.04.035.
Xiang, Y., Zhu, Z., Han, G., Lin, H., Xu, L., Chen, C.D., 2007. JMJD3 is a histone H3K27 demethylase. Cell Res. 17, 850–857. http://dx.doi.org/10.1038/cr.2007.83.
Ye, L., Qiu, L., Zhang, H., Chen, H., Jiang, C., Hong, H., Liu, J., 2016. Cardiomyocytes in young infants with congenital heart disease: a three-month window of proliferation. Sci. Rep. 6, 23188. http://dx.doi.org/10.1038/srep23188.
Zhang, F., Xu, L., Xu, L., Xu, Q., Li, D., Yang, Y., Karsenty, G., Chen, C.D., 2015. JMJD3 promotes chondrocyte proliferation and hypertrophy during endochondral bone formation in mice. J. Mol. Cell Biol. 7, 23–34. http://dx.doi.org/10.1093/jmcb/mjv003.
Zhou, Y., Cashman, T.J., Nevis, K.R., Obregon, P., Carney, S.A., Liu, Y., Gu, A., Mosimann, C., Sondalle, S., Peterson, R.E., Heideman, W., Burns, C.E., Burns, C.G., 2011. Latent TGF-β binding protein 3 identifies a second heart field in zebrafish. Nature 474, 645–648. http://dx.doi.org/10.1038/nature10094.